Supplementary information for

"Quantifying the rigidity of 2D carbide (MXenes)"

Tao Hu[a,b], Jinxing Yang[b,c], Wu Li[d], and Xiaohui Wang[b,*], and Changming Li[a,e]

[a]Institute of Materials Science and Devices, Suzhou University of Science and Technology, Suzhou 215009, China

[b]Shenyang National Laboratory for Materials Science, Institute of Metal Research, Chinese Academy of Sciences, 72 Wenhua Road, Shenyang 110016, China

[c]University of Science and Technology of China, Hefei 230026, China

[d]Institute for Advanced Study, Shenzhen University, Shenzhen 518060, China

[e]Institute for Cross-field Science and College of Life Science, Qingdao University, Qingdao 200671, China.

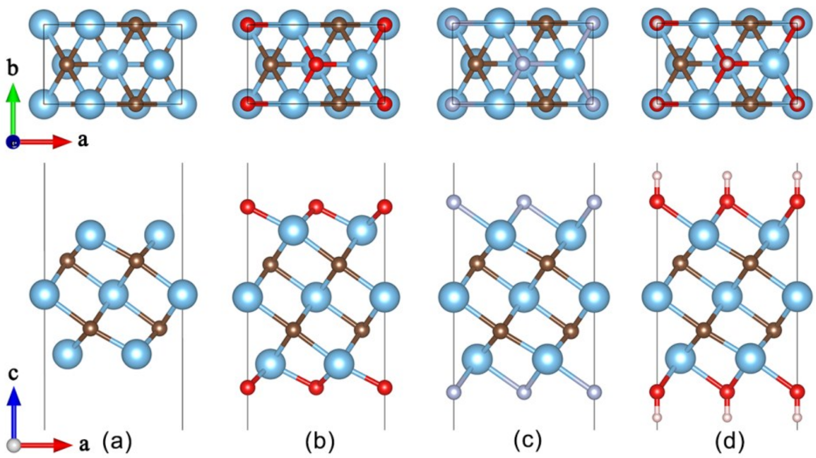

Fig. S1 Atomic geometries of rectangular cell of $Ti_3C_2T_2$ MXenes. (a) Ti_3C_2 (b) $Ti_3C_2O_2$ (c) $Ti_3C_2F_2$ and (d) $Ti_3C_2(OH)_2$

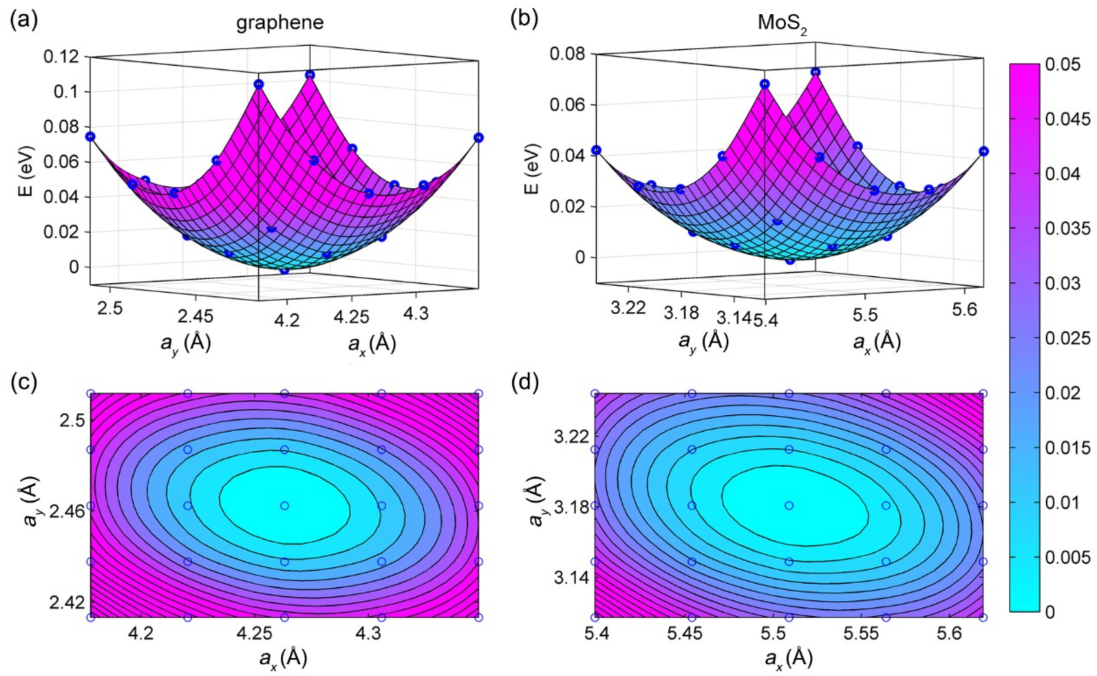

Fig. S2 The three-dimensional plot of a_x, a_y and corresponding strain energies of (a) graphene and (b) MoS_2. Contour of energy in the a_x–a_y plane of (c) graphene and (d) MoS_2. For graphene, C = 337.8744 N/m. This value is in a good agreement with earlier experimental and theoretical study. Our calculated value of the in-plane stiffness of graphene is in good agreement with the experimental value of 340 ± 50 N/m and justifies the reliability of our method. For MoS_2, C =122.4 N/m, agrees well with reported value of 123 N/m

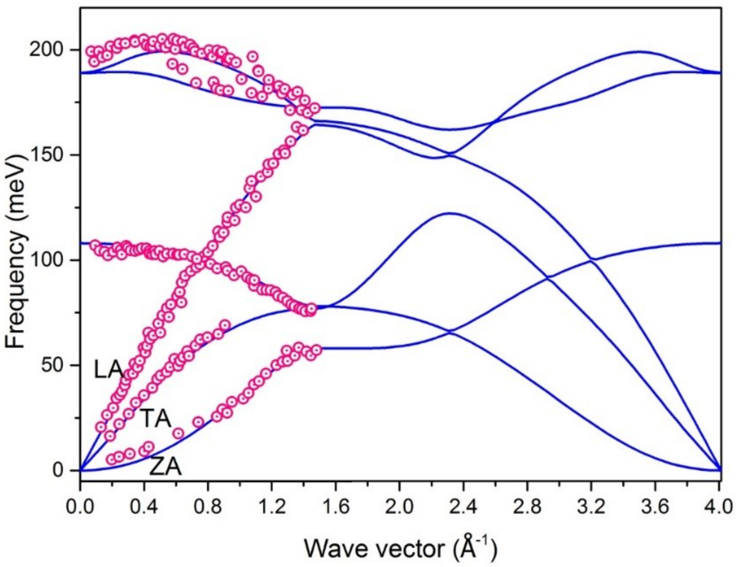

Fig. S3 Calculated phonon dispersion in this work and experimental phonon dispersion of monolayer graphene by high-resolution electron energy loss spectroscopy[1]

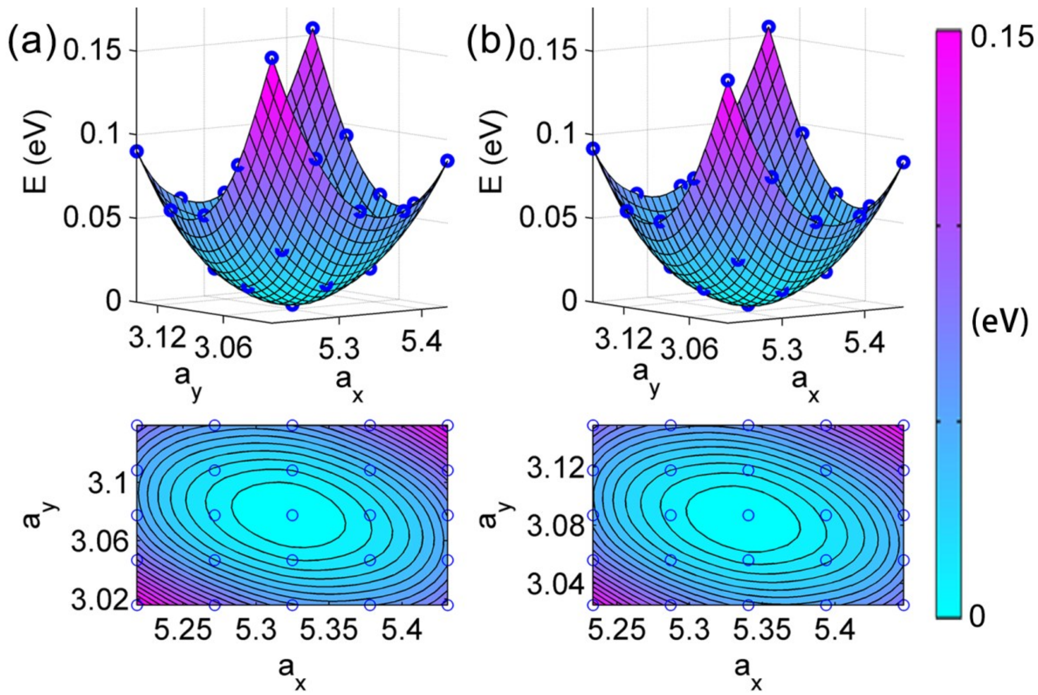

Fig. S4 Energy surface of strained monolayer $Ti_3C_2T_2$ MXenes for the calculation of in-plane stiffness. The three-dimensional plot of a_x, a_y and corresponding strain energies and contour of energy in the a_x–a_y plane of (a) $Ti_3C_2F_2$ and (b) $Ti_3C_2(OH)_2$. The blue balls are based on calculation and the lines are the fitted formula. Note that the stiffness increases by functionalization in Ti_3C_2 MXenes

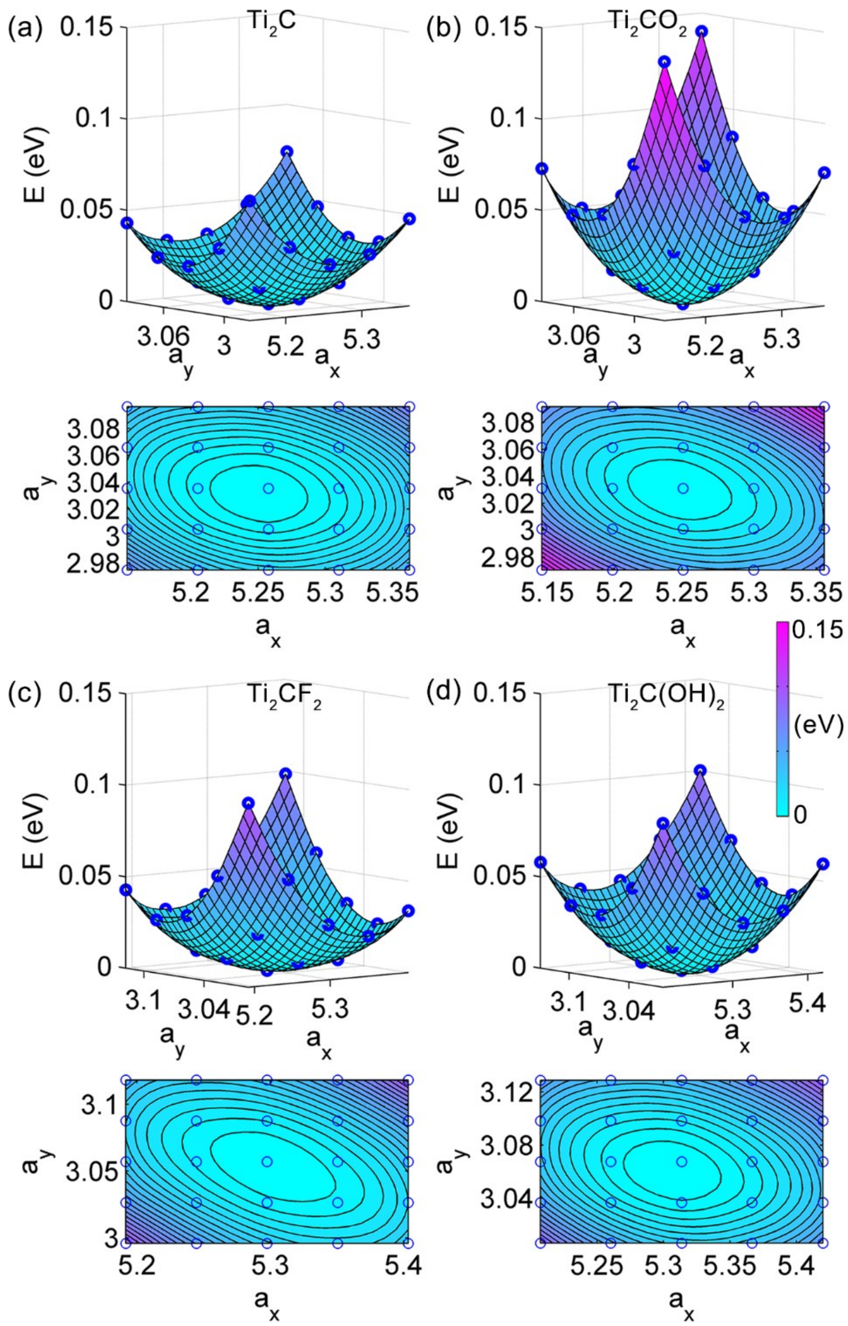

Fig. S5 Stiffness of monolayer Ti_2CT_2 MXenes. The three-dimensional plot of a_x, a_y and corresponding strain energies and contour of energy in the $a_x - a_y$ plane of (a) Ti_2C, (b) Ti_2CO_2, (c) Ti_2CF_2, and (d) $Ti_2C(OH)_2$. The blue balls are actual points and the lines are the fitted formula. Note that the stiffness increases by functionalization in Ti_2C MXenes

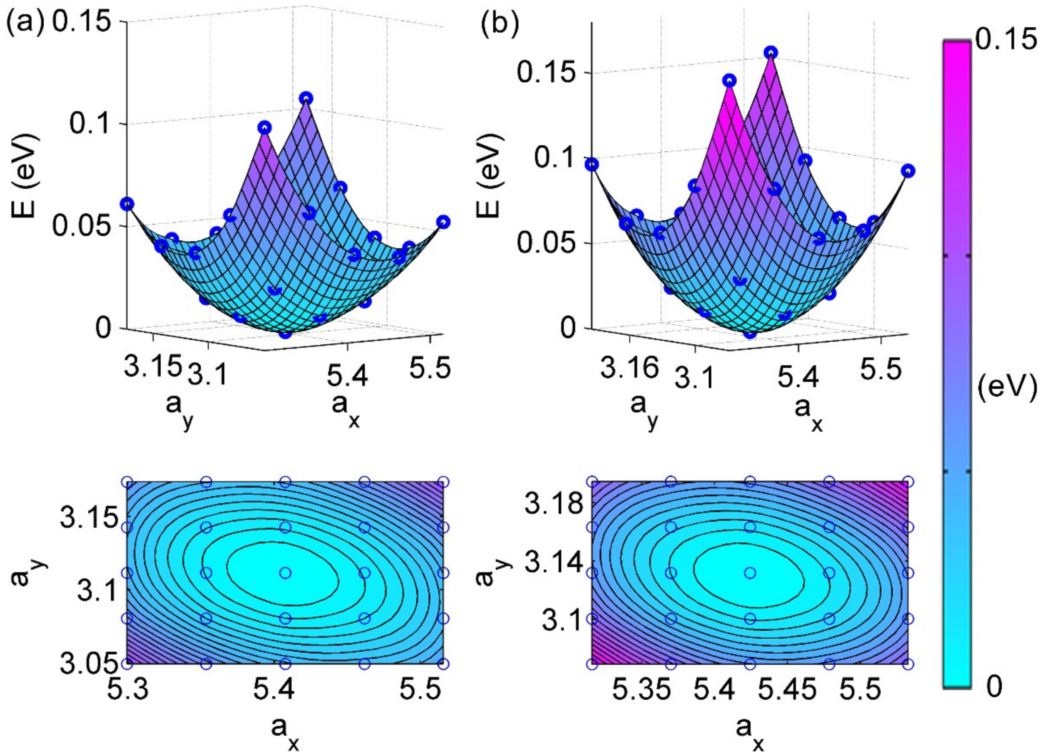

Fig. S6 Stiffness of monolayer Nb_2C and Nb_2CO_2 MXenes. The three-dimensional plot of a_x, a_y and corresponding strain energies and contour of energy in the $a_x - a_y$ plane of (a) Nb_2C, and (b) Nb_2CO_2. The blue balls are actual points and the lines are the fitted formula. Note that the stiffness increases by functionalization in Nb_2C MXenes

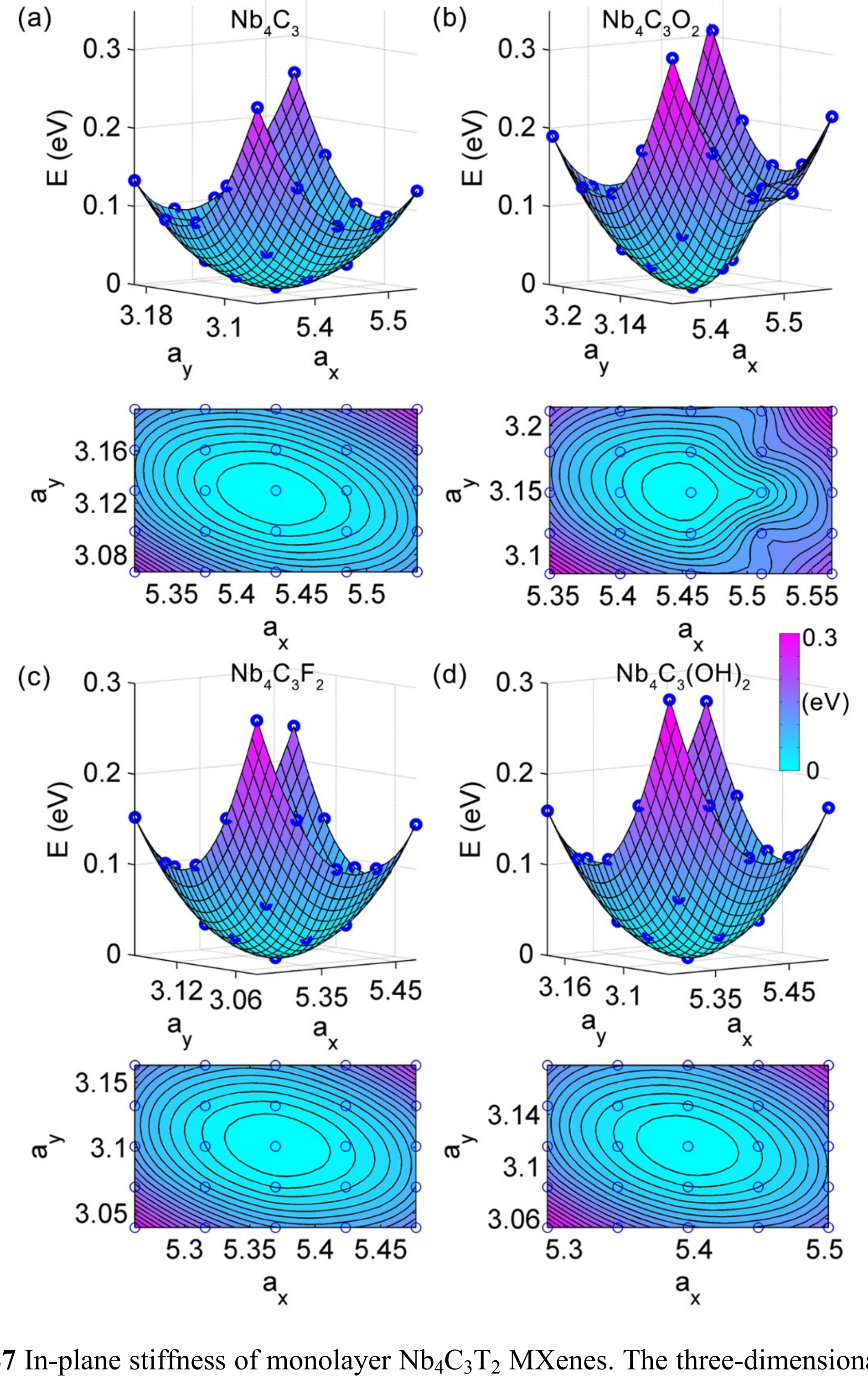

Fig. S7 In-plane stiffness of monolayer $Nb_4C_3T_2$ MXenes. The three-dimensional plot of a_x, a_y and corresponding strain energies, and contour of energy in the $a_x - a_y$ plane of (a) Nb_4C_3, (b) $Nb_4C_3O_2$, (c) $Nb_4C_3F_2$, and (d) $Nb_4C_3(OH)_2$. The lengths of a_x, a_y are in Å

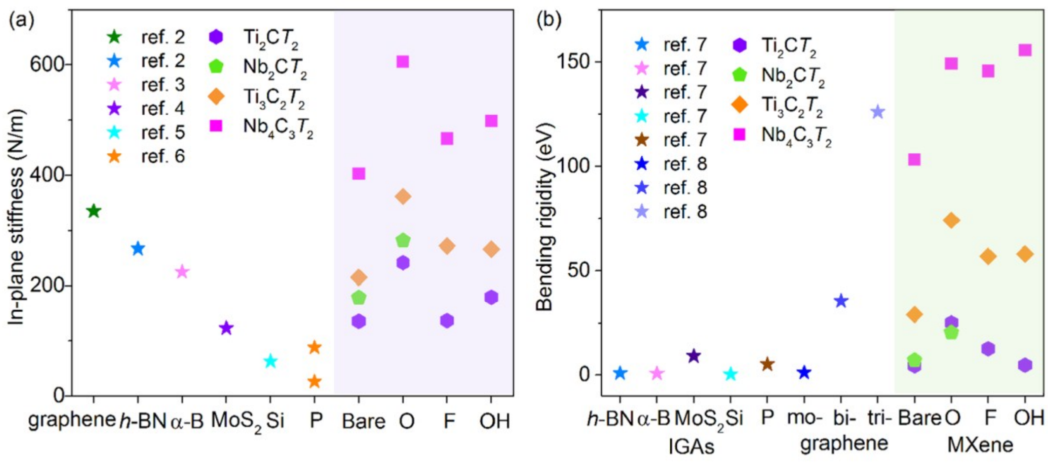

Fig. S8 (a) In-plane stiffness and (b) bending rigidity of MXenes and other typical 2D materials. In-plane stiffness of graphene [2], *h*-BN [2], Borophene [3], MoS_2 [4], Silicene [5], phosphorene [6] and out-of-plane bending rigidities [7,8] are collected from literature

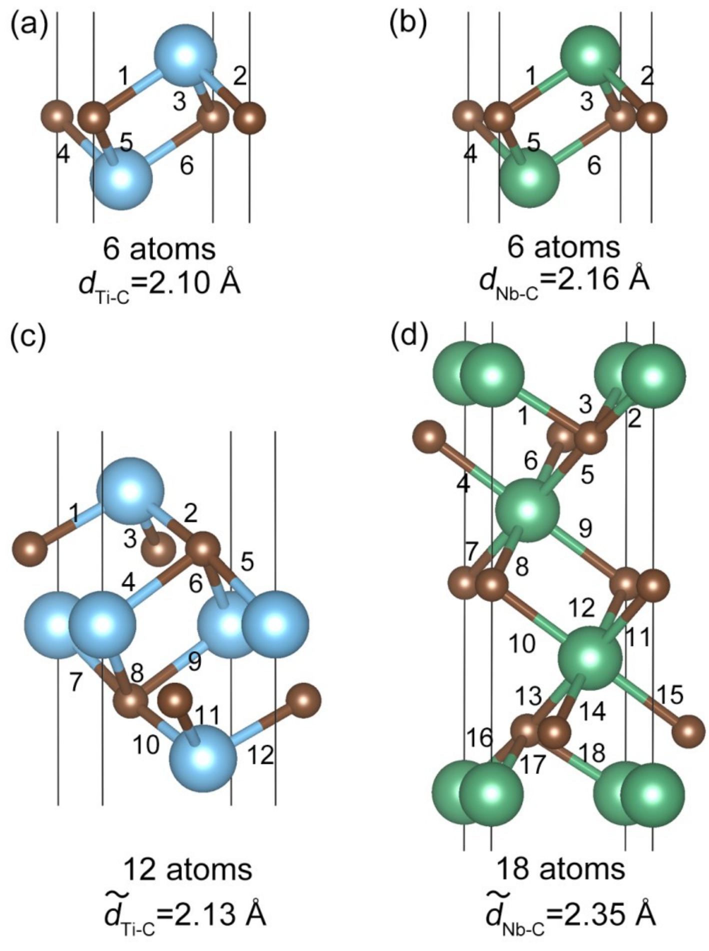

Fig. S9 Schematic of number of M-C bonds and average M-C bond lengths in (a) Ti_2C, (b) Nb_2C, (c) Ti_3C_2, and (d) Nb_4C_3 MXenes.

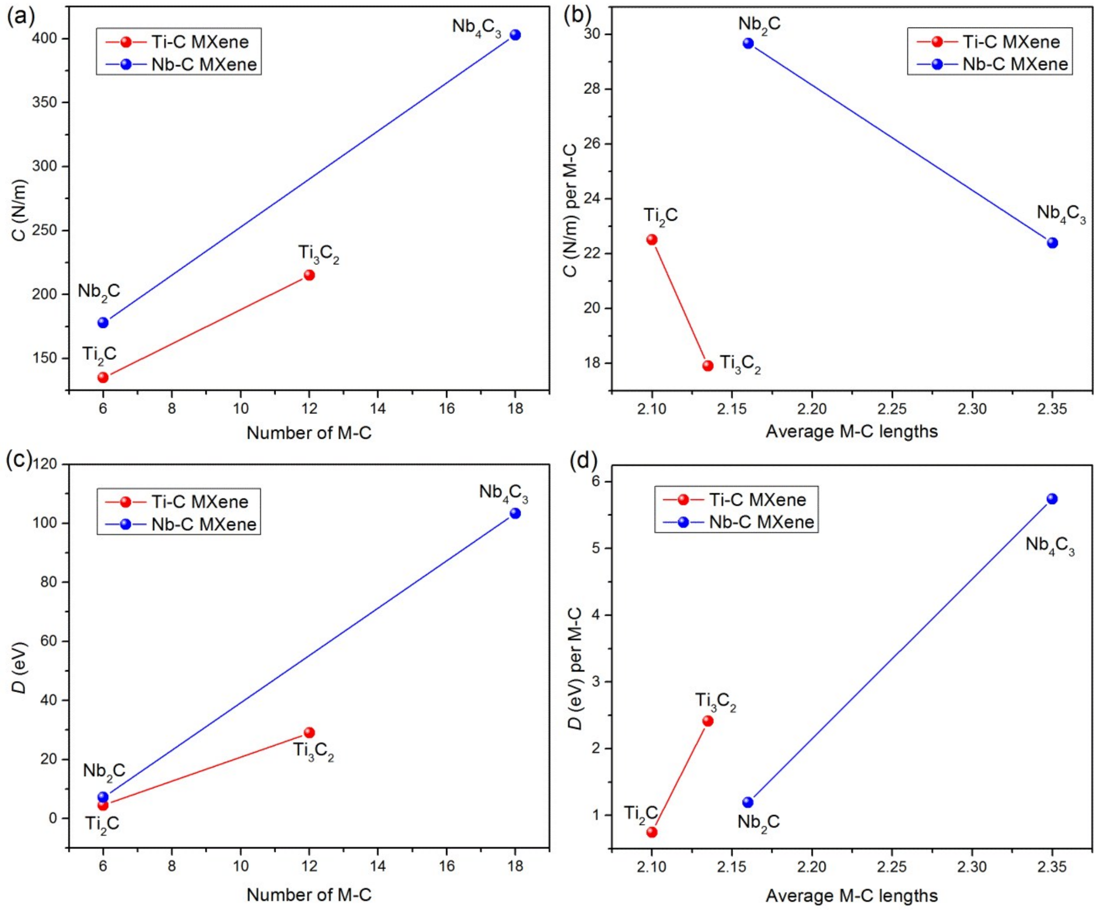

Fig. S10 In-plane stiffness C and bending rigidity D versus number of M-C and average M-C bond lengths. The thickness-dependence of in-plane stiffness in MXenes can also be easily understood at microscopic scale if the chemical bonds are considered. The covalent/ionic mixing bonds M-C constitute the basic framework of MXenes considering the nearest neighbors. Increasing [$M_{n+1}X_n$] layer thickness means increasing the number of M-C bonds, and thus increasing the in-plane stiffness. The [$M_{n+1}X_n$] layer as the substrate provides the basic stiffness. Then the functional groups strengthen to different extents.

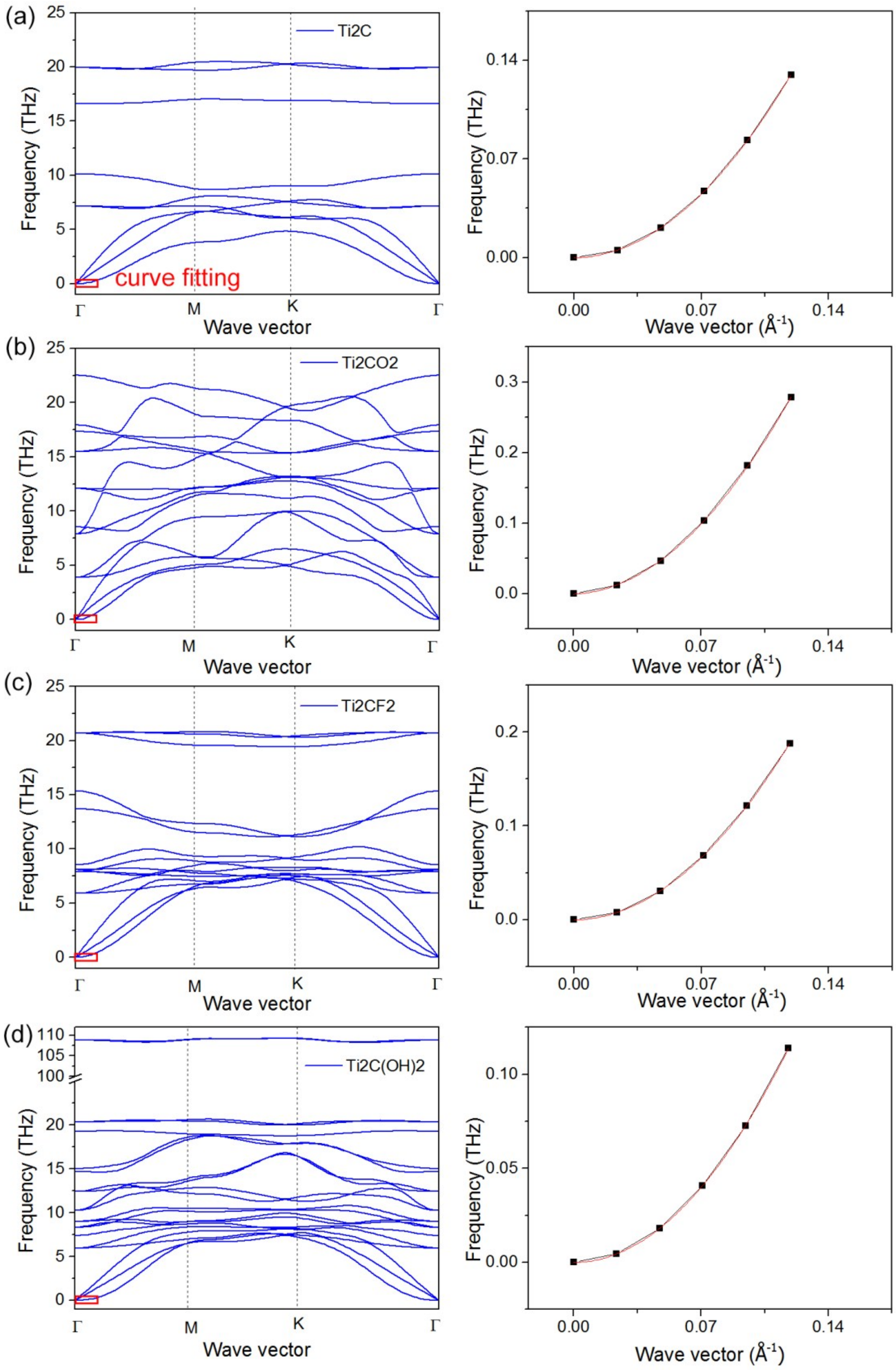

Fig. S11 phonon dispersion and curve fitting details of Ti_2CT_2 MXenes.

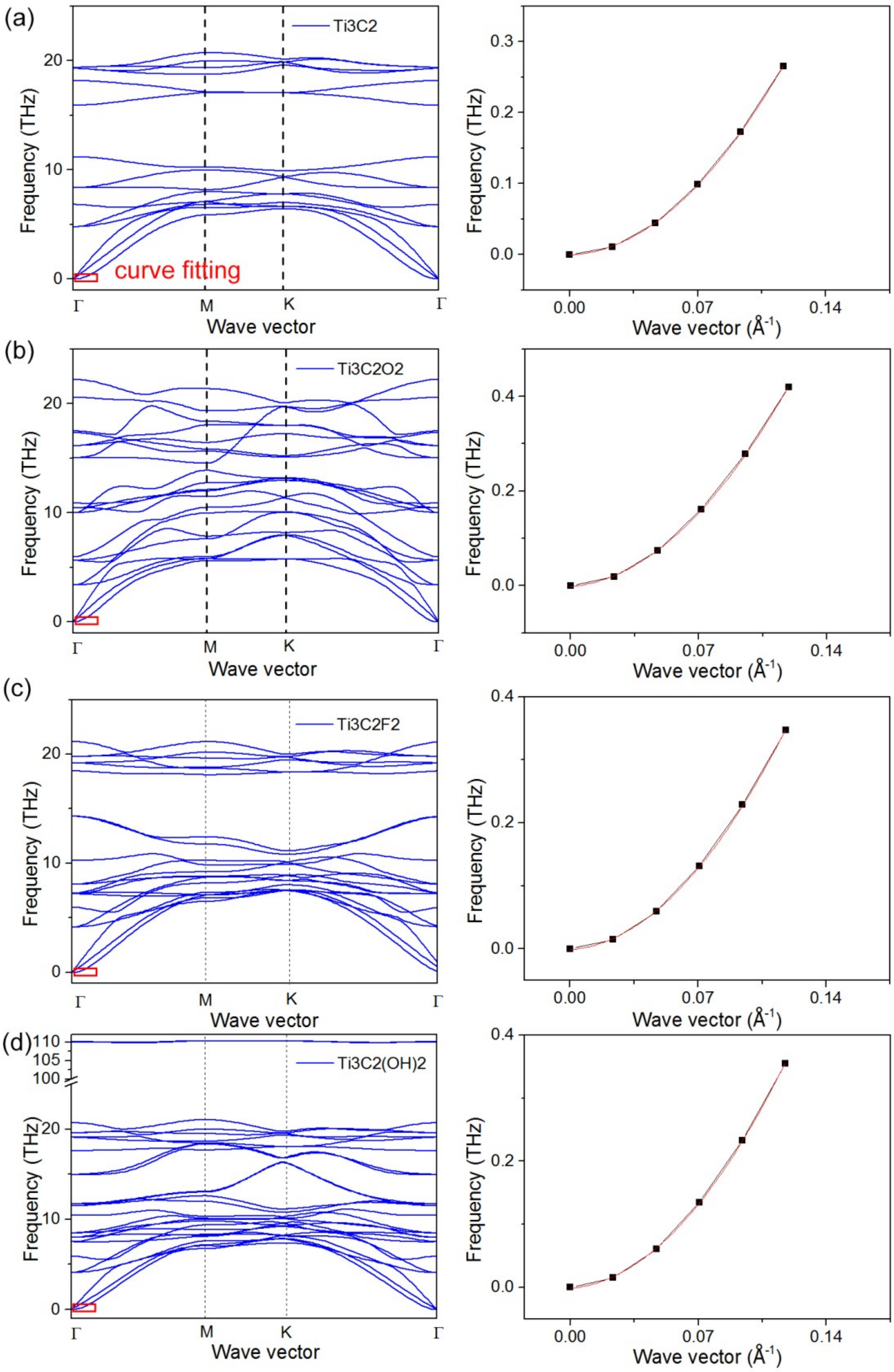

Fig. S12 phonon dispersion and curve fitting details of $Ti_3C_2T_2$ MXenes.

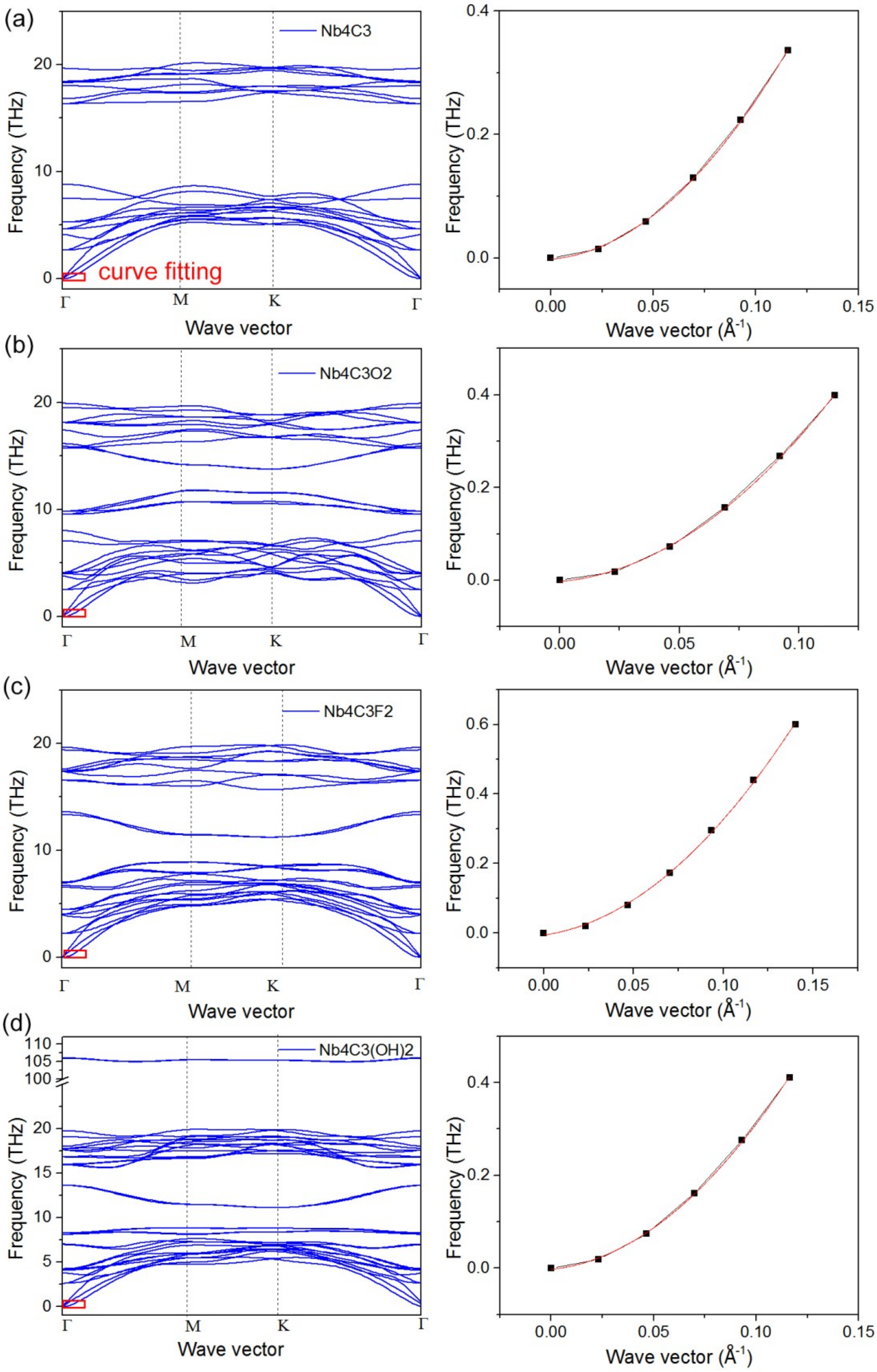

Fig. S13 phonon dispersion and curve fitting details of $Nb_4C_3T_2$ MXenes.

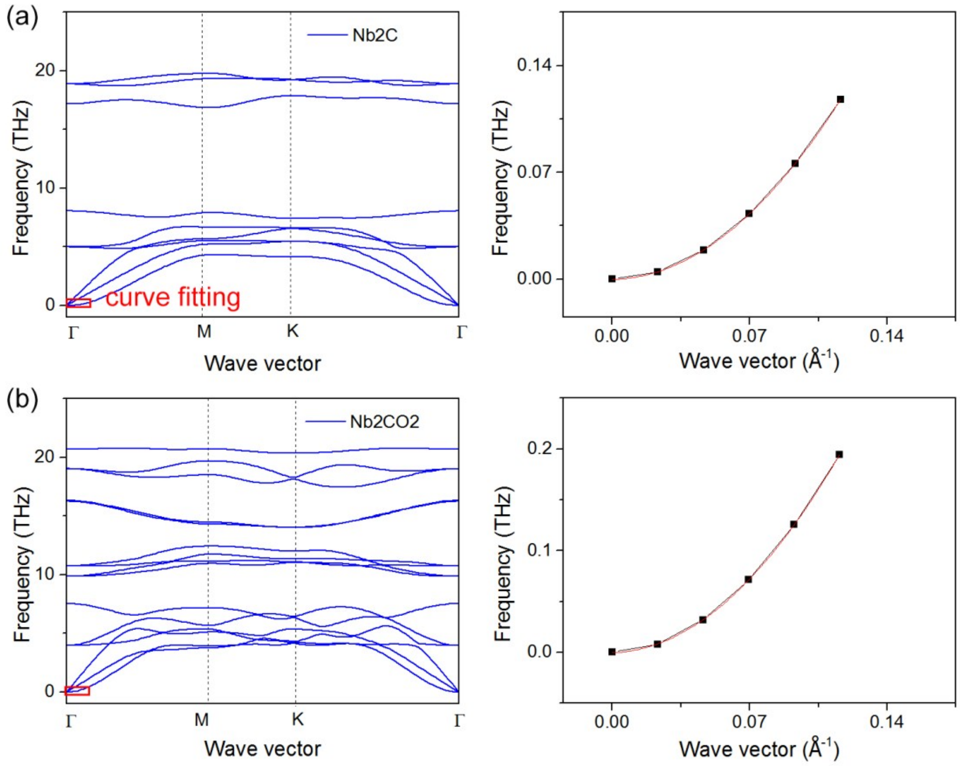

Fig. S14 phonon dispersion and curve fitting details of Nb_2C and Nb_2CO_2 MXenes.

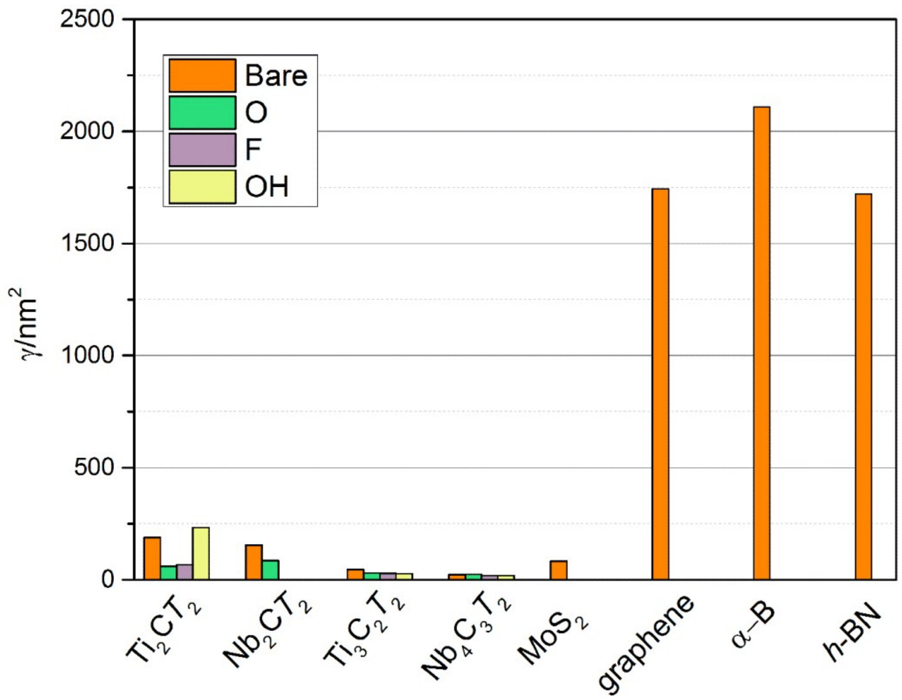

Fig. S15 Foppl-von Karman number per unit area of MXenes and typical 2D materials. γ of MXenes is much lower than that of single-atom-thick graphene. Available data in the literature demonstrates the reliability of this study

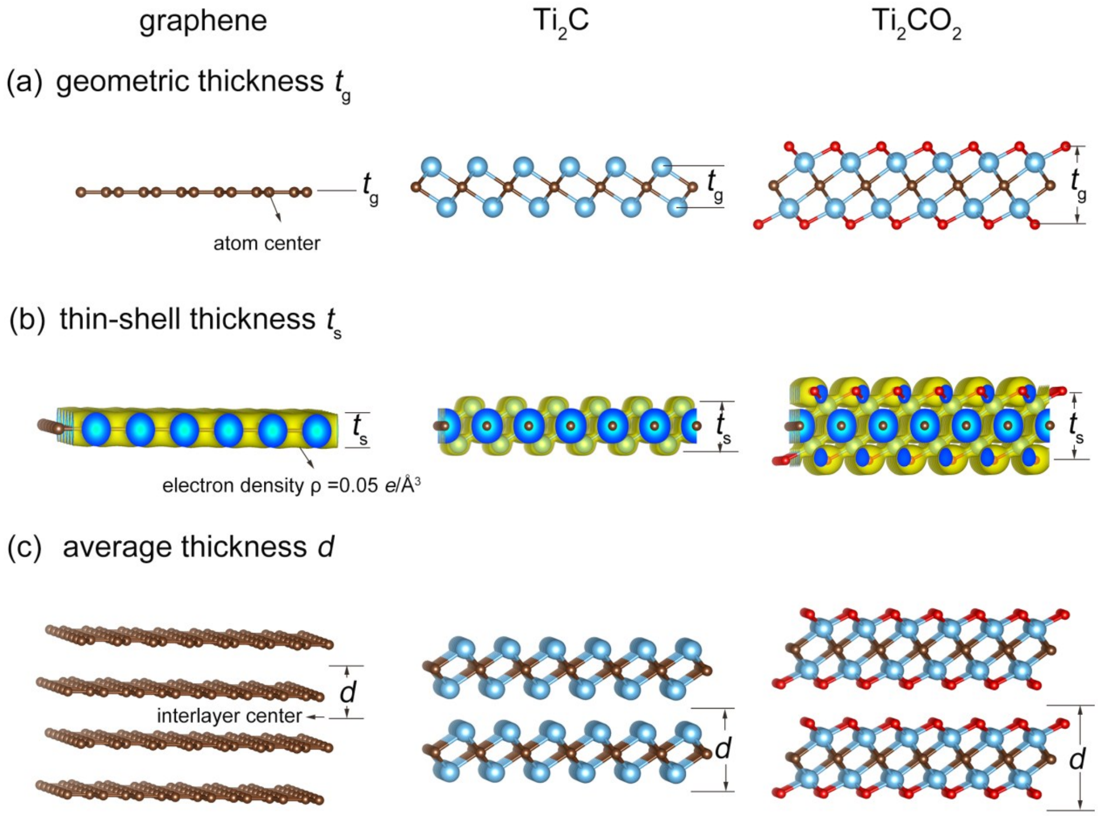

Fig. S16 Schematic of (a) geometric thickness t_g, (b) thin-shell thickness t_s, and (c) average thickness *d*. Compared with geometric thickness, electrons contribute to the thickness in the thin-shell thickness like 'glue'. Isosurface of electron density of 0.05 e/Å^3 is presented in (b)

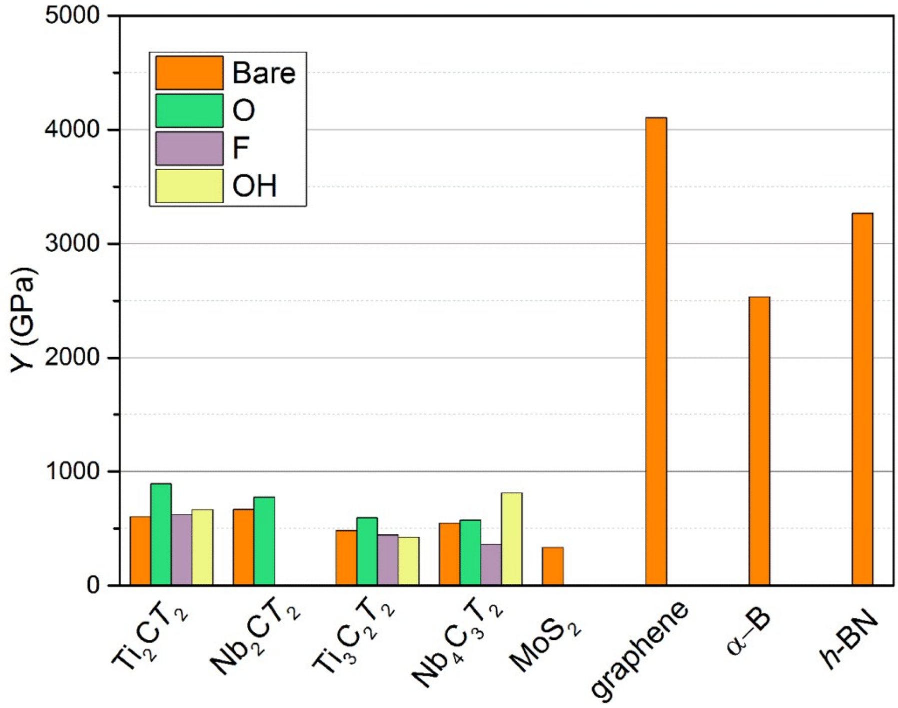

Fig. S17 Young's moduli Y of MXenes and typical 2D materials. We note that the Young's modulus of graphene calculated by $Y = C/t_s$ is 4.1 TPa, about four-fold of 1.0 TPa, which was obtained assuming effective thickness equal to average layer thickness of graphite 3.35 Å.[9] By more accurate micro Raman spectroscopy measurement, Young's modulus of graphene was estimated to be more than 2 TPa.[10] The ultrahigh Young's modulus of graphene is attributed to the lack of σ bond participation under bending.[11] And the authors pointed out that the plate phenomenology is filled in multilayer (number of layer N=3 with only 6% error). As the ambiguous nature of thickness of atomic thick materials, in-plane stiffness is more appropriate parameter than the Young's modulus.

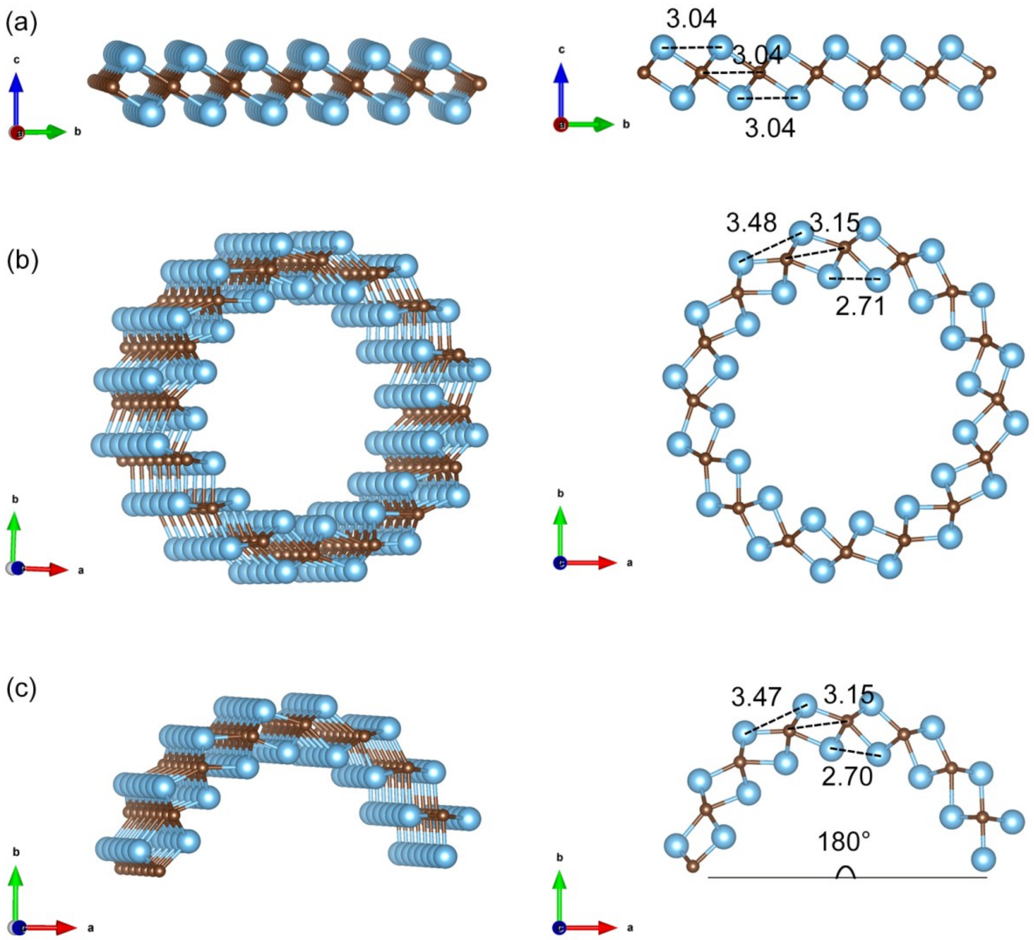

Fig. S18 Optimized structures of (a) Ti_2C MXene monolayer, a 6×6 supercell (b) A Ti_2C (8, 8) nanotube with 48 atoms/unit cell (c) A Ti_2C sheet bend to 180 semi-tube, with C atoms fixed while relaxing Ti atoms. Note that the bent MXenes behaviors like a plate, with uniform deformation, involving extension on the convex while compression on the concave side. The result shows that the shell generally satisfy the glued interfaces and thus follows the $D{\sim}N^3$ (N represents number of atomic layers) relationship.[12] For MXene, we did not observe the lubricated sliding. Instead, the uniform deformation is observed in MXene. The outer diameter and inner diameter of the optimized Ti_2C (8, 8) nanotube are 16.0 Å and 11.5 Å respectively, in good agreement with earlier work.[13]

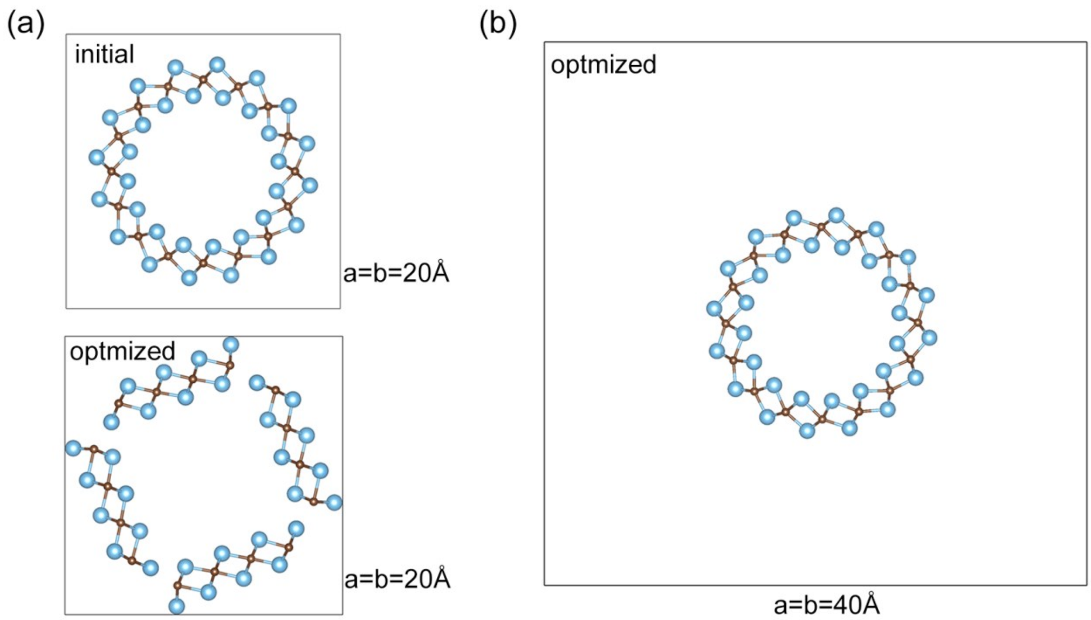

Fig. S19 Structural optimization of Ti_2C (8, 8) nanotube with 48 atoms/unit cell with (a) a 20.00 Å × 20.00 Å × 3.03 Å box, and (b) 40.00 Å × 40.00 Å × 3.03 Å box. By using sufficient large box like 40.00 Å × 40.00 Å × 3.03 Å box, the disintegration of tubular structure into a bundle of nanostripes, which is also observed in Ti_2C (ref. [14]) and Sc_2C (ref. [15]) did not occur.

Table S1. A summary of parameters fitted through the energy−strain curved surface of monolayer MXenes

MXenes	c_1	c_2	c_3
Ti_2C	70.32	73.63	30.26
Ti_2CO_2	133.70	46.12	85.15
Ti_2CF_2	86.48	46.12	77.58
$Ti_2C(OH)_2$	97.17	94.45	46.12
Ti_3C_2	114.90	123.10	114.90
$Ti_3C_2O_2$	193.50	189.1	103.8
$Ti_3C_2F_2$	151.00	156.00	84.87
$Ti_3C_2(OH)_2$	147.00	152.80	77.12
Nb_4C_3	238.10	241.40	153.00
$Nb_4C_3O_2$	335.80	269.40	120.90
$Nb_4C_3F_2$	259.60	255.10	133.80
$Nb_4C_3(OH)_2$	281.70	279.00	151.80
Nb_2C	102.30	103.90	59.86
Nb_2CO_2	157.90	157.00	73.55
graphene	114.50	114.90	40.95
MoS_2	71.35	72.31	35.57

Table S2. Theoretical in-plane stiffness *C*, out-of-plane bending rigidity *D*, Foppl-von Karman number per unit area, γ, effective shell thickness t_s, average layer thickness *d*, and geometric layer thickness t_g of MXenes and typical 2D materials. Note that the Termination-Termination interaction within one layer is quite weak, that they contribute little to the thickness of the shell in functionalized MXenes. This is in agreement with the [$M_{n+1}X_n$] provide the framework and basic in-plane stiffness.

formula	*C* (N/m)	*D* (eV)	γ (nm^{-2})	*ν*	t_s (Å)	*d* (Å)	t_g (Å)
Ti_2C	135.53	4.47	189.50	0.21	2.46	4.86	2.30
Ti_2CO_2	241.86	25.02	60.42	0.32	4.22	6.77	4.42
Ti_2CF_2	136.67	12.65	67.52	0.45	3.76	6.95	4.78
$Ti_2C(OH)_2$	179.12	4.81	232.74	0.24	2.20	8.84	6.73
Nb_2C	178.13	7.17	155.27	0.29	2.66	4.93	2.36
Nb_2CO_2	281.65	20.45	86.08	0.23	3.63	6.89	4.64
Ti_3C_2	214.85	28.99	46.32	0.50	4.41	7.35	4.63
$Ti_3C_2O_2$	361.42	74.29	30.41	0.27	6.05	9.29	8.94
$Ti_3C_2F_2$	271.93	56.95	29.84	0.28	6.09	9.35	7.21
$Ti_3C_2(OH)_2$	266.05	58.08	28.63	0.26	6.25	9.64	9.22
Nb_4C_3	402.59	103.34	24.35	0.32	6.65	10.26	7.59
$Nb_4C_3O_2$	605.99	149.15	25.39	0.18	6.76	12.60	9.82
$Nb_4C_3F_2$	466.38	145.65	20.01	0.26	7.48	13.31	10.65
$Nb_4C_3(OH)_2$	497.97	155.70	19.99	0.27	7.46	14.25	12.52
MoS_2	123	9.14	84.11	0.25	3.66	6.15	3.12
graphene	335	1.20	1744.79	0.18	0.82	3.34	0

Table S3 Optimized multilayer structures by PW91-OBS scheme in the determination of average layer thickness *d*. For Ti_2CT_2 and Nb_2CT_2, one unit cell includes only one layer, while for $Ti_3C_2T_2$ and $Nb_4C_3T_2$, one unit cell includes 2 layers.

formula	Stacking type	*c* (Å)	*d* (Å)
Ti_2C	Bernal	4.86	4.86
Ti_2CO_2	Bernal	6.77	6.77
Ti_2CF_2	Bernal	6.95	6.95
$Ti_2C(OH)_2$	Bernal	8.84	8.84
Nb_2C	Bernal	4.93	4.93
Nb_2CO_2	Bernal	6.89	6.89
Ti_3C_2	Bernal	14.70	7.35
$Ti_3C_2O_2$	Bernal	18.58	9.29
$Ti_3C_2F_2$	Bernal	18.70	9.35
$Ti_3C_2(OH)_2$	Bernal	19.28	9.64
Nb_4C_3	Bernal	20.52	10.26
$Nb_4C_3O_2$	Bernal	25.20	12.60
$Nb_4C_3F_2$	Bernal	26.62	13.31
$Nb_4C_3(OH)_2$	Bernal	28.50	14.25
MoS_2	Bernal	12.30	6.15
graphene	Bernal	6.68	3.34

Average layer thickness is calculated based on the most stable multilayer stacking structures of MXenes. Like graphene stack into graphite in Bernal stacking configuration, homogeneously terminated MXenes energetically favor Bernal stacking, as demonstrated in the earlier work[16].

Derivation of bending rigidity from ZA phonon branches:

The bending rigidity of 2D materials deriving from ZA branches of phonon dispersion is described in an easy to understand in the review paper of graphene.[17] In part III of this paper (Page 132-133), authors talked about flexural phonons, elasticity, and crumpling of graphene. We make extracts below. They started from the elastic energy:

$$E_0 = \frac{\kappa}{2}\int d^2r(\nabla \cdot N)^2 \approx \frac{\kappa}{2}\int d^2r(\nabla^2 h)^2 , \quad \text{(S1)}$$

Where κ is the bending rigidity and h is the height variable. r is the in-plane vector and N is the unit vector normal to the surface.

Then rewrite in momentum space as:

$$E_0 = \frac{\kappa}{2}\sum_k k^4 h_{-k} h_k . \quad \text{(S2)}$$

Then canonically quantize the problem by introducing a momentum operator P_k that has the following commutator with h_k:

$$\left[h_k, P_{k'}\right] = i\delta_{k,k'} , \quad \text{(S3)}$$

And Hamiltonian as

$$H = \sum_k \{\frac{P_{-k}P_k}{2\sigma} + \frac{\kappa k^4}{2} h_{-k} h_k\} , \quad \text{(S4)}$$

Where σ is 2D mass density. From the Heisenberg equations of motion for the operators, it is trivial to find that h_k oscillates harmonically with a frequency given by

$$\omega_{flex}(k) = (\frac{\kappa}{\sigma})^{1/2} k^2 . \quad \text{(S5)}$$

Which is the long-wavelength dispersion of flexural modes. The bending rigidity κ is related with flexural modes frequencies by the above equation.

Details of data processing.

The fitted function from data in **Fig. 4a** is as following:

MXenes:

$$D = 0.3741C - 52.8394 \tag{S6}$$

Effective thickness < 1 angstrom, graphene, h-BN, α-B

$$D = 0.0044C - 0.2514 \tag{S7}$$

The fitted function from data in **Fig. 4b** is as following:

$$\gamma = 8.6679 - 74.0043t_s^{-1} + 1227.3120t_s^{-2} \tag{S8}$$

$$D = -6.2497 + 12.0250t_s - 4.7626t_s^2 + 0.8122t_s^3 \tag{S9}$$

Reference

[1] A. Politano, A. R. Marino, D. Campi, D. Farías, R. Miranda and G. Chiarello, *Carbon*, 2012, **50**, 4903.

[2] M. Topsakal, S. Cahangirov and S. Ciraci, *Appl. Phys. Lett.*, 2010, **96**, 091912.

[3] Q. Peng, L. Han, X. Wen, S. Liu, Z. Chen, J. Lian and S. De, *Phys. Chem. Chem. Phys.*, 2015, **17**, 2160.

[4] Q. Yue, J. Kang, Z. Shao, X. Zhang, S. Chang, G. Wang, S. Qin and J. Li, *Phys. Lett. A*, 2012, **376**, 1166.

[5] R. Qin, C.-H. Wang, W. Zhu and Y. Zhang, *AIP Advances*, 2012, **2**, 022159.

[6] M. Elahi, K. Khaliji, S. M. Tabatabaei, M. Pourfath and R. Asgari, *Phys. Rev. B*, 2015, **91**, 115412.

[7] Z. Zhang, Y. Yang, E. S. Penev and B. I. Yakobson, *Adv. Funct. Mater.*, 2017, **27**, 1605059.

[8] N. Lindahl, D. Midtvedt, J. Svensson, O. A. Nerushev, N. Lindvall, A. Isacsson and E. E. Campbell, *Nano Lett.*, 2012, **12**, 3526.

[9] C. Lee, X. D. Wei, J. W. Kysar and J. Hone, *Science*, 2008, **321**, 385.

[10] J. U. Lee, D. Yoon and H. Cheong, *Nano Lett.*, 2012, **12**, 4444.

[11] D. B. Zhang, E. Akatyeva and T. Dumitrica, *Phys. Rev. Lett.*, 2011, **106**, 255503.

[12] G. Wang, Z. Dai, J. Xiao, S. Feng, C. Weng, L. Liu, Z. Xu, R. Huang and Z. Zhang, *Phys. Rev. Lett.*, 2019, **123**.

[13] X. Guo, P. Zhang and J. Xue, *J Phys Chem Lett*, 2016, **7**, 5280.

[14] A. N. Enyashin and A. L. Ivanovskii, *Comput. Theor. Chem.*, 2012, **989**, 27.

[15] X. Zhang, Z. Ma, X. Zhao, Q. Tang and Z. Zhou, *J. Mater. Chem. A*, 2015, **3**, 4960.

[16] T. Hu, M. M. Hu, Z. J. Li, H. Zhang, C. Zhang, J. Y. Wang and X. H. Wang, *Phys. Chem. Chem.*

Phys., 2016, **18**, 20256.
[17] A. H. C. Neto, F. Guinea, N. M. R. Peres, K. S. Novoselov and A. K. Geim, *Reviews of Modern Physics*, 2009, **81**, 109.